

VIP **Ionic Crystals** Very Important Paper
How to cite: *Angew. Chem. Int. Ed.* **2022**, *61*, e202208247

International Edition: doi.org/10.1002/anie.202208247

German Edition: doi.org/10.1002/ange.202208247

sp² to sp³ Hybridization Transformation in Ionic Crystals under Unprecedentedly Low Pressure

 HPSTAR
 1536-2022

Xingxing Jiang, Maxim S. Molokeev, Naizheng Wang, Yonggang Wang,* Ting Wen, Zhichao Dong, Youquan Liu, Wei Li,* and Zheshuai Lin*

Abstract: Under cold pressure sp¹/sp²-to-sp³ hybridization transformation has been exclusively observed in covalent or molecular crystals overwhelmingly above ≈10 GPa, and the approaches to lower the transition pressure are limited on external heat-treatment and/or catalyzers. Herein we demonstrate that, by internal-lattice stress-transfer from ionic to covalent groups, the transformation can be significantly prompted, as shown in a crystal of LiBO₂ under 2.85 GPa for the first case in ionic crystals. This unprecedentedly low transformation pressure is ascribed to the enhanced localized stress on covalent B–O frames transferred from ionic Li–O bonds in LiBO₂, and accordingly the corresponding structural feature is summarized. This work provides an internal structural regulation strategy for pressure-reduction of the s-p orbital hybridization transformation and extends the sp¹/sp²-to-sp³ transformation landscape from molecular and covalent compounds to ionic systems.

extended carbon monoxide.^[3] The s-p hybridization always occurs during the formation of covalent bonds, so previous studies were mainly focused on interatomic interactions of purely covalent or molecular compounds with covalent bonds. Owing to the strong directionality and saturation of covalent bonds, modifications of their direction and coordination number for the s-p hybridization transformation must overcome large energy barriers; at room temperature, the transition pressures are often very high,^[1a,2-4] and some of them are even higher than one hundred GPa.^[4a] This poses a serious challenge for current high-pressure experimental technology. At present, pressures below ≈30 GPa can be realized with a mature large-volume-press apparatus, but the cost increases sharply with increasing pressure. On the other hand, a pressure above ≈30 GPa is typically realized with diamond anvil cell technology. Due to the small chamber, the diamond anvil cell can only be used with trace samples, which restricts low-cost and large-scale preparation of materials with densified structures. Therefore, it is highly desirable to lower the pressures required for sp¹/sp²-sp³ transformations.

Based on the use of state-of-the-art high-pressure equipment, external controlling approaches, such as applying high temperatures and/or introducing catalyzers, have been developed to reduce the pressures required for sp¹/sp²-to-sp³ transformations. For example, the pressure required for the sp²-to-sp³ transformation from graphite to diamond can be reduced from ≈15 GPa to ≈5 GPa by high-treatment at ≈1000 °C and/or addition of metal catalyzers,^[5] and a high-temperature treatment at ≈1500 °C realized the transforma-

Introduction

The pressure-induced transformation from sp¹/sp² to sp³ hybridization is an important way to densify the structures of compounds and achieve intriguing physicochemical properties, such as superhardness in diamond,^[1] superconductivity in solid-state carbon disulfide^[2] and ultrahigh energy density in

[*] Dr. X. Jiang, N. Wang, Y. Liu, Prof. Z. Lin
 Functional Crystals Lab, Technical Institute of Physics and Chemistry, Chinese Academy of Sciences
 Beijing 100190 (China)
 E-mail: zslin@mail.ipc.ac.cn

Dr. X. Jiang, Prof. Z. Lin
 Center of Materials Science and Optoelectronics Engineering, University of Chinese Academy of Sciences
 Beijing 100049 (China)

Dr. M. S. Molokeev
 Laboratory of Crystal Physics, Kirensky Institute of Physics, SB RAS
 Krasnoyarsk 660036 (Russia)

and
 Department of Physics, Far Eastern State Transport University
 Khabarovsk 680021 (Russia)
 and
 Siberian Federal University
 Krasnoyarsk 660041 (Russia)

Prof. Y. Wang
 School of Materials Science and Engineering, Peking University
 Beijing 100871 (China)
 E-mail: ygw@pku.edu.cn

Dr. T. Wen
 Center for High Pressure Science & Technology Advanced Research
 Beijing 100094 (China)

Dr. Z. Dong
 Laboratory of Space Astronomy and Technology, National Astronomical Observatories, Chinese Academy of Sciences
 Beijing 100101 (China)

Prof. W. Li
 School of Materials Science and Engineering, TKL of Metal and Molecule-Based Material Chemistry, Nankai University
 Tianjin 300350 (China)
 E-mail: wl276@nankai.edu.cn

N. Wang, Y. Liu, Prof. Z. Lin
 University of Chinese Academy of Sciences
 Beijing 100049 (China)

tion from sp^2 -hybridized fullerene to sp^3 -hybridized amorphous carbon with unexpected hardness at ≈ 30 GPa.^[6]

Here, we propose another avenue to reduce sp^1/sp^2 -to- sp^3 transformation pressures, i.e., by introducing ionic bonds into the coordination structures of compounds. Unlike covalent bonds, ionic bonds do not exhibit directionality and saturation. We assume that if ionic bonds are connected to sp^1/sp^2 -hybridized covalent groups with certain structural arrangements, their coordination modes could be adjusted under pressure and the stress transferred onto the nearby covalent groups to enhance the local stress in the covalent groups and promote sp^1/sp^2 -to- sp^3 transformations (see Figure 1). If this is verified, it would provide an internal-structure regulating strategy to reduce the transformation pressures of s-p hybridizations.

To demonstrate the above concept, we concentrated on borate crystals. This is because the boron-oxygen group is one of the fundamental covalent groups in which both threefold (sp^2 -hybridized) and fourfold (sp^3 -hybridized) coordination patterns (i.e., $[BO_3]$ and $[BO_4]$, respectively) can exist at ambient pressure.^[7] In fact, although it has never been discovered in borate crystals, an sp^2 -to- sp^3 transformation in borate glass was identified via in situ local structure analysis under high pressure.^[8] Since there are thousands of borate crystals, the covalent B–O groups have many modes with which to interact with the ionic groups, so it should be possible to find suitable candidates for our purpose. Herein, we identify lithium metaborate ($LiBO_2$) as the first ionic crystal that manifests a sp^2 -to- sp^3 transformation during a pressure-induced phase transition. Synchrotron radiation high-pressure powder X-ray diffraction (PXRD) experiments revealed that this transformation occurred at cold temperatures and an unprecedentedly low pressure of 2.85 GPa, which was confirmed by high-pressure Raman and infrared spectra combined with first-principles simulations. The structural requirements for reducing the pressures of sp^2 -to- sp^3 transformations in ionic crystals are then proposed. In the sp^2 -to- sp^3 transformation, $LiBO_2$ exhibited a large reduction in unit cell volume of 22 %, and the incompressibility of the high-pressure (HP-) $LiBO_2$ phase was comparable with that of diamond. The mechanism for the low pressure sp^2 -to- sp^3

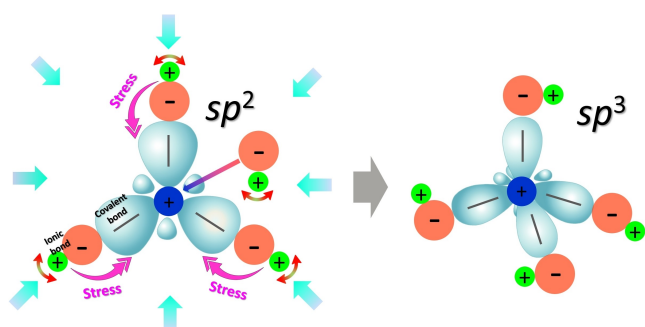


Figure 1. Schematic for the concept of stress-transfer engineering in ionic crystals. Under pressure (represented by the light blue arrows), benefiting from nondirectionality and unsaturation, the coordination pattern of ionic bonds could be adjusted to transfer the in-lattice stress onto nearby covalent groups to promote the sp^2 -to- sp^3 transformation.

transformation was elucidated, and the optical, dielectric and Li-migration properties of the high-pressure $LiBO_2$ phase are also predicted.

Results and Discussion

At ambient pressure, $LiBO_2$ (low pressure $LiBO_2$, LP- $LiBO_2$) crystallizes in the monoclinic $P2_1/c$ space group, with the cell parameters $a = 5.8275(9)$ Å, $b = 4.3454(5)$ Å, $c = 6.4661(10)$ Å, $\beta = 114.5563(62)^\circ$, and $V = 148.931(37)$ Å³. As depicted in Figure 2a, each boron atom in LP- $LiBO_2$ is sp^2 -hybridized with three oxygen atoms forming a $[BO_3]$ triangle, and the $[BO_3]$ triangles are connected to one another along the b -axis by sharing oxygen atoms to form infinite one-dimensional (1D) covalent $\{[BO_3]_n\}$ chains (Figure 2b). The lithium atoms are coordinated with four oxygen atoms from neighboring $\{[BO_3]_n\}$ chains to form ionic $[LiO_4]$ tetrahedra. Furthermore, the covalent $\{[BO_3]_n\}$ chains and ionic $[LiO_4]$ tetrahedra are alternatively arranged along the a -axis, and a three-dimensional (3D) framework structure is constructed (Figure 2b and c). It should be emphasized that since there are no atoms located in the interstices between the $\{[BO_3]_n\}$ chains along the c -axis (Figure 2c), distortions of the ionic Li–O polyhedra under pressure could make the $\{[BO_3]_n\}$ chains approach each other and produce strong interactions, which could induce the sp^2 -to- sp^3 transformation.

The high-pressure PXRD patterns observed for $LiBO_2$ below 2.85 GPa at room temperature revealed that, except for peak shifts to high angles, no peaks emerged or disappeared, indicating that the LP-phase structure was well

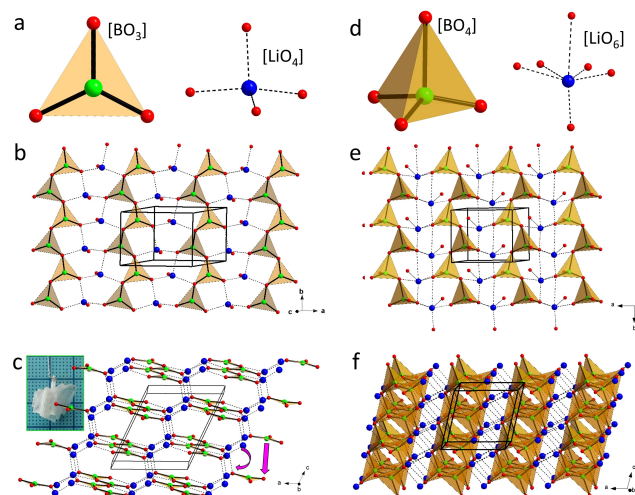


Figure 2. Crystal structures of LP- and HP- $LiBO_2$. a) $[BO_3]$ and $[LiO_4]$ groups. b) viewed along the c -axis and c) viewed along the b -axis for LP- $LiBO_2$. The inset displays the as-grown crystal, and the approaches of B and O atoms accounting for the sp^2 -to- sp^3 transformation and the coupling adjustment of Li–O coordination are indicated by pink arrows. d) $[BO_4]$ and $[LiO_6]$ groups. e) viewed along the c -axis and f) viewed along the b -axis for HP- $LiBO_2$. The Li, B and O atoms are represented by blue, green and red balls, respectively. The covalent B–O and ionic Li–O bonds are represented by solid and dashed lines, respectively, and the unit cells are represented by black parallelepipeds.

maintained. Starting from 2.85 GPa, new peaks at 7.02° and 16.91° emerged (Figure 3a and Figure S1a). Moreover, the peaks at 15.75°, 16.42°, 17.49° and 17.81° gradually merged, and their intensities were enhanced with increasing pressure. These results demonstrated that a new phase (named high-pressure LiBO₂, HP-LiBO₂) was formed, and its proportion became increasingly prominent as the pressure was increased. The phase-transition process lasted at pressures up to 8.13 GPa, at which point the compound was entirely converted to HP-LiBO₂. Above 8.13 GPa, the XRD patterns, except for peak-shifting, did not change, suggesting that the high-pressure phase was well formed. To determine the structure of HP-LiBO₂, the PXRD pattern at the highest measured pressure (15.0 GPa) was used, since the HP-LiBO₂ phase had the highest purity under this condition. Through an elaborate process, the structure of HP-LiBO₂ was shown to have the same space group (*P2₁/c*) and *Z* (4) value as LP-LiBO₂ with the cell parameters *a*=5.1506(27) Å, *b*=4.3921(12) Å, *c*=4.9155(9) Å, *β*=103.829(67)°, and *V*=107.975(71) Å³. The atomic positions and bond lengths for HP-LiBO₂ at 15.0 GPa are listed in Tables S1, S2.^[9] The phonon spectrum calculation of the crystal structure of HP-LiBO₂ at 15 GPa revealed that no imaginary frequency was detected, suggesting the dynamical stability of the solved structure (Figure S4). In comparison with the open framework of the LP phase, the high-pressure structure of LiBO₂ was changed to a densified 3D network structure by converting the planar groups ([BO₃]) in the low-pressure structure to tetrahedral groups ([BO₄]) and by altering the ionic Li–O coordination from four- to sixfold (Figure 2d). By sharing corner oxygen atoms, the [BO₄] moieties were connected with each other to form two-dimensional (2D) {–[BO₄]}_∞ layers, which are further adhered by the ionic [LiO₆] octahedra to form the 3D structure (Figure 2e and f). Both the experimental PXRD patterns at ≈0 GPa and 15 GPa were well fitted with the LP- and HP-LiBO₂ structures, respectively (see Figure 3b and 3c, as well as the patterns in Figure S2). From the structural

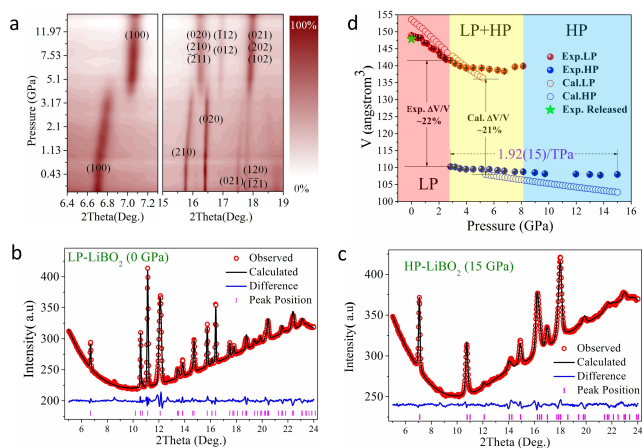


Figure 3. High-pressure PXRD data, lattice volume variations of LiBO₂. a) Evolution of PXRD patterns for LiBO₂. b) and c) Rietveld refinement plots for LP- and HP-LiBO₂ at ≈0 GPa and 15 GPa, respectively. d) Evolution of lattice volume with respect to pressure for LP- and HP-LiBO₂.

comparison, one may easily determine the structural evolution involved during conversion of the LP- to HP-phase in LiBO₂: when compressed by pressure, the neighboring {–[BO₃]}_∞ chains in the LP-phase structure gradually approached each other along the *c*-axis (see Figure 2c), which eventually led to formation of interchain B–O bonds and induced the sp²-to-sp³ transformation with construction of 2D {–[BO₄]}_∞ layers in HP-LiBO₂ (Figure 2f). When pressure was unloaded, the PXRD pattern reverted to that of the low-pressure phase, and the cell parameters also reverted to the initial values, indicating that the sp²-to-sp³ transformation in LiBO₂ is fully reversible (Figure 3d, Figure S1b and S3).

To confirm that the pressure-induced transition was accompanied by sp²-to-sp³ transformation, we carried out high-pressure infrared (IR) and Raman studies with maximum pressures of 14.9 GPa and 12.4 GPa, respectively. To eliminate external interference as much as possible, no pressure-transmitting medium was used during data collection. It is well known that the [BO₃] and [BO₄] groups in borates can be identified by peaks located in the wavenumber ranges 1300–1500 cm⁻¹ and 700–1200 cm⁻¹ in the Raman and IR spectra, respectively.^[10] The pressure-dependent IR spectra showed that the peak at approximately 1500 cm⁻¹ faded, while that at approximately 1000 cm⁻¹ was enhanced, with increasing pressure (Figure 4a), which verified the conversion from [BO₃] to [BO₄] during the LP- to HP-LiBO₂ transition. The high-pressure Raman spectra also showed that the peak at 1470 cm⁻¹, which represents the stretching vibrations of B–O bonds in [BO₃] groups, decreased in intensity with increasing pressure (Figure 4b), and a peak at approximately 1190 cm⁻¹ (representing [BO₄]) emerged at 2.9 GPa and increased in intensity up to the maximum pressure applied (12.4 GPa), confirming the gradual conversion from [BO₃] to [BO₄] groups in LiBO₂. On the other hand, a new Raman peak at ≈550 cm⁻¹ emerged at 1.9 GPa, and its intensity increased as the pressure was increased (Figure 4b). Since the characteristic frequencies for the stretching vibrations of Li–O bonds are approximately 400–600 cm⁻¹,^[11] this clearly indicated that the Li–O coordination mode was modified during the phase transition. In addition, when the pressures were unloaded, both the high-pressure IR and Raman spectra reverted to those seen at ambient pressure (see Figure 4a and

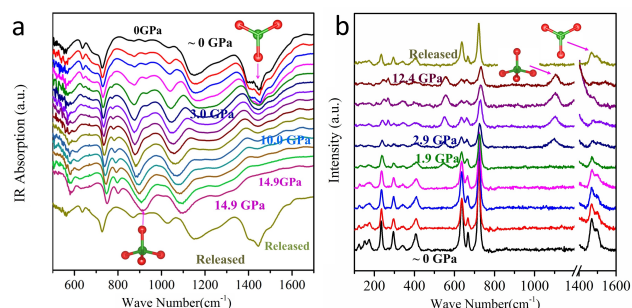


Figure 4. High-pressure infrared and Raman spectra of LiBO₂. a) Evolution of IR spectra versus pressure. The small peak at ≈0 GPa for amorphous [BO₄] came from the residue produced during solid-state synthesis. b) Evolution of Raman spectra versus pressure.

b, as well as Figure S5, which shows the variations in intensities and frequencies for the IR peaks at $\approx 1500\text{ cm}^{-1}$ and at $\approx 1000\text{ cm}^{-1}$. This observation confirmed that the sp^2 to sp^3 transformation was perfectly reversible for both B–O coordination and B–O bond lengths in the LiBO_2 crystal. This differed somewhat from the situation in borate glass, in which, although the B–O coordination transformation was reversed, the changes in B–O bond lengths were irreversible.^[8b] We also calculated the IR and Raman spectra for both LP- and HP- LiBO_2 phases via a first-principles method; these were in good agreement with the experimental data (see Figure S6), verifying the validity of the resolved crystal structures and the occurrence of the $[\text{BO}_3]$ to $[\text{BO}_4]$ transformation.

Note that the critical pressure of 2.85 GPa for the sp^2 -to- sp^3 transformation in LiBO_2 was much lower than those for all known compounds, including graphite (≈ 15 GPa, room temperature),^[4f] BN (≈ 14 GPa, room temperature),^[4d] CO_2 (above 40 GPa, 1800 K),^[4b] CS_2 (40–50 GPa, room temperature),^[2] CO (7.1 GPa, room temperature),^[3] and N_2 (≈ 110 GPa, above 2000 K),^[4a] as plotted in Figure S7. To understand the underlying mechanism for the unprecedentedly low sp^2 -to- sp^3 transformation pressure, we performed finite element method (FEM) simulations of the structures for LP- and HP- LiBO_2 . In the FEM simulations, the crystal structures were modeled with ball-stick models, in which the mechanical moduli of the components were characterized by the linear harmonic oscillator approximation based on the Raman spectrum (see details in the “Finite Element Analysis” section in Supporting Information). The simulations revealed that in both LP- and HP- LiBO_2 , the B–O framework had very small distortions under pressure, and the strain was mainly localized on the Li–O polyhedra (Figure 5a and b). In contrast, most of the stress was concentrated on the B–O framework, while the ionic Li–O bonds almost did not participate in the stress resistance (Figure 5c and d). This means that the distorted Li–O polyhedra transferred their stress onto the nearby covalent B–O framework and generated very high local stress on the latter, which effectively reduced the macroscopic pressure required for the sp^2 -to- sp^3 transformation. Moreover, the first-principles charge-density distributions (Figure 5e and f) show that prominent electron delocalization occurred around the B–O groups during the sp^2 -to- sp^3 transformation, whereas the charge densities around the Li–O bonds remained almost unchanged, even though the coordination of Li was significantly modified from fourfold to sixfold. Since electron delocalization under pressure corresponds to a pressure-induced energy-storage process,^[12] this suggests that formation of additional covalent B–O bonds from $[\text{BO}_3]$ to $[\text{BO}_4]$ accounted for the energy stored during the phase transition. In comparison, owing to their nondirectional character, the Li–O bonds relatively easily adjusted to release of the pressure-induced energy. Thus, the energy (in the form of stress) from the ionic Li–O polyhedra was transferred onto the B–O groups to prompt the sp^2 -to- sp^3 transformation, and the energy consumed (and the critical pressure) for the phase transition in LiBO_2 was significantly reduced. Indeed, as shown in Figure 5g, the total energy difference between the

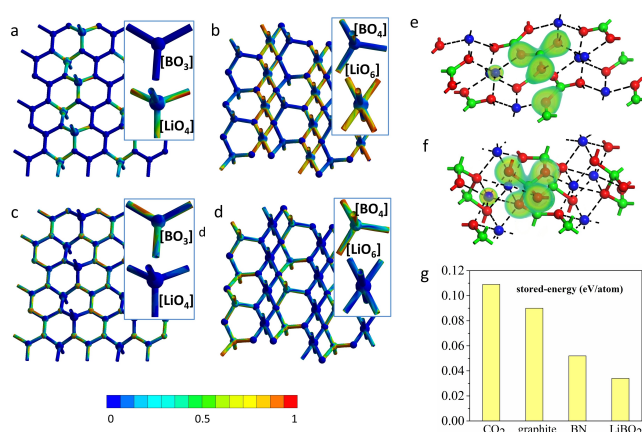


Figure 5. Mechanism for the sp^2 - sp^3 transformation in LiBO_2 . FEM simulation results for strain distributions in a) LP- and b) HP- LiBO_2 and stress distributions in c) LP- and d) HP- LiBO_2 . The magnified distributions of the basic structural units, $[\text{BO}_3]$ and $[\text{LiO}_4]$ in LP- and $[\text{BO}_4]$ and $[\text{LiO}_6]$ in HP-models, are displayed in the insets. Electronic charge density distributions in e) LP- and f) HP- LiBO_2 . Note that the charge densities were calculated for the extended lattices with periodic boundary conditions. To clearly display the charge distributions before and after the phase transition, only those around one unit, i.e., one B–O group and Li ions, are plotted. Lithium, boron and oxygen atoms are represented by blue, green and red balls, respectively. Li–O bonds are represented by black dashed lines. g) Energy differences between sp^1/sp^2 -hybridized and sp^3 -hybridized phases in crystals for which the structures are known.

HP- and LP- LiBO_2 structures at the phase transition point was much smaller than those of all other compounds for which both sp^2 - and sp^3 -hybridized crystal structures are known (including carbon dioxide,^[4c] graphite^[1b] and boron nitride^[4d]).

According to the above analysis, one may summarize the structural features that enable the sp^1/sp^2 -to- sp^3 hybridization transformation under pressure in an ionic crystal as follows: (i) the microscopic structure should be constructed to make the sp^1/sp^2 -hybridized covalent groups and ionic groups alternatively arranged in the crystal framework; (ii) the coordination numbers and bond directions within the ionic groups should be susceptible to modification under pressure; and (iii) there should be no atoms located in the interstices among the covalent units along at least one direction. In this way, the stress on ionic bonds can be directly transferred to the nearby covalent units to prompt the sp^1/sp^2 -to- sp^3 transformation under a much smaller critical pressure. It should be emphasized that this model is based on internal-lattice structure regulation, which is absolutely different from models based on external condition control.^[13]

Although it is known that the sp^2 -to- sp^3 transformation can give rise to prominent structural densification, the pressure-induced volume collapse in LiBO_2 was unexpectedly large. As shown in Figure 3d, the variations of both PXRD-refined and theoretically calculated cell parameters for the LP- to HP- LiBO_2 phases with respect to pressure clearly illustrated a large volume collapse (ΔV) with experimental and calculated magnitudes of $\approx 22\%$ and $\approx 21\%$, respectively, at the phase-transition points (an experimental value

of 2.85 GPa and a theoretical value of 5 GPa, as displayed in Figure S8). This collapse magnitude is among the largest known for pressure-induced phase transitions, including graphite to diamond ($\approx 27\%$),^[4f] hexagonal h-BN to cubic c-BN ($\approx 21\%$),^[4d,14] and molecular nitrogen to singly bonded cg-N (25%).^[4a] Such large lattice densification was also observed during formation of another high-pressure LiBO₂ phase (γ -phase) synthesized under high-temperature and high-pressure conditions ($\approx 23\%$ densification, which was not explicitly pointed out by the authors).^[15] Our detailed structural analyses of the experimental structures showed that the newly formed B–O bonds in the sp²-to-sp³ transformation were almost within the (*a*, *c*) plane, which caused the area of the (*a*, *c*) plane to decrease from 32.69 Å² in LP- to 25.10 Å² in HP-LiBO₂ (by 23 %, Table S3), which was almost of the same magnitude as the volume collapse (22 %). In comparison, the cell parameter along the *b*-axis remained almost constant (only increasing by approximately 1 %, Table S3). Therefore, the substantial pressure-induced structural densification in LiBO₂ is predominantly ascribed to modification of the coordination environment from [BO₃] to [BO₄] due to the sp²-to-sp³ transformation along the *c*-axis. Remarkably, the fitted volume compressibility of HP-LiBO₂ is 1.92(15)/TPa, which is comparable with the compressibility magnitudes for diamond (≈ 2.2 /TPa),^[16] c-BN (≈ 2.5 /TPa),^[17] ReB₂ (≈ 2.7 /TPa),^[18] BC₂N (≈ 3.54 /TPa)^[19] and osmium (the most incompressible material in nature, ≈ 2.16 /TPa).^[20] The ultrastrong incompressibility of HP-LiBO₂ is attributed to the densified lattice structure resulting from the large volume collapse driven by the sp²-to-sp³ transformation.

The structural densification caused by the sp²-to-sp³ transformation can also result in the enhancement of optical, dielectric and Li-migrating properties of LiBO₂. The first-principles electronic band structures (Figure S9) showed that the band gap energies of LP- and HP-LiBO₂ are 7.1 eV and 8.3 eV, which corresponds to ultraviolet adsorption edges of 175 nm and 149 nm, respectively, in good agreement with the UV–vis diffuse reflection measurement of the LP phase (< 200 nm,^[21] and the value for the HP phase is not available owing to the limit of the apparatus). Enlargement of the transparent range for HP-LiBO₂ is attributed to the energy gap for the frontier orbitals in the [BO₄] groups, which is larger than that for the [BO₃] groups.^[7] Moreover, we predict that the dielectric permittivity at zero frequency (ϵ_0) for HP-LiBO₂ is 8.46, an increase of approximately 60 % compared with that of LP-LiBO₂ ($\epsilon_0 = 5.30$, Table S7), which, combined with the high resistance resulting from the wide band gap, would favor applications in dielectric devices. Since LiBO₂ contains lithium ions, we also theoretically investigated Li migration in the material. The calculated barrier for migration of lithium ions in LP-LiBO₂ was 0.56 eV, consistent with the available experimental values (0.21–0.23 eV, 0.30 eV and 0.71–0.80 eV).^[22] For HP-LiBO₂, we predict that the Li-migration barrier will be reduced to 0.40 eV because B–O sp³ hybridization saturated the electronic charge on oxygen, which in turn weakened the Li–O interaction (the average bond valence of the Li–O bond was reduced from 0.24 in LP-LiBO₂ to 0.18 in HP-LiBO₂) during the transition. As a result, the lithium-ion conductivity at room temperature would be

increased by approximately 470 times on going from LP- to HP-LiBO₂ because the ion mobility is proportional to $e^{-q/KT}$, where *q*, *K* and *T* are the migration barrier, Boltzmann constant and temperature, respectively.^[23]

Conclusion

In summary, by using internal-lattice stress-transfer engineering of ionic bonds, we discovered LiBO₂ as the first ionic crystal that exhibits a pressure-induced sp²-to-sp³ transformation under low pressure. This transformation occurred under a very low critical pressure of 2.85 GPa and is accompanied by a large unit cell collapse of 22 %. The unprecedentedly low transition pressure for LiBO₂ is ascribed to the localized stress transferred onto the covalent B–O framework from the nondirectional ionic Li–O bonds, which was also confirmed from the viewpoint of energy storage, thus providing a fundamental understanding of the structural evolution of ionic crystals under pressure. Accordingly, the structural features required to enable a low critical pressure for sp¹/sp²-to-sp³ transformations in ionic crystals were suggested, i.e., (i) an alternating arrangement of the sp¹/sp²-hybridized covalent groups and ionic groups, (ii) ionic groups apt to modify their coordination geometry under pressure, and (iii) no atom located among the covalent groups along at least one direction. Benefitting from the densified atomic packing induced by the sp²-to-sp³ transformation, HP-LiBO₂ is expected to exhibit intriguing physicochemical properties, including ultrastrong incompressibility, large dielectric permittivity and high lithium-ion conductivity. This work provides an internal-structure approach for regulating the critical pressure reductions of s-p orbital hybridization transformations and extends sp¹/sp²-sp³ hybridization transformations from molecular and covalent crystals to ionic crystals. This is believed to have significant implications for new high-pressure chemistry, which would open up an avenue through which to explore high-pressure syntheses of new materials. Interestingly, numerous minerals, especially ionic salt compounds, are condensed into sp³-hybridized fourfold coordinated structures in the crust and upper mantle in the Earth, where the pressure is well below ten GPa.^[24] Elucidation of the mechanism for sp¹/sp²-sp³ transformations in ionic crystals, as presented in this work, may also be beneficial in understanding the formation of solid matter during geological and planetary evolution.

Acknowledgements

The authors acknowledge Zhuohong Yin for useful discussions and the experimental time provided by the 4W2 beam line of the Beijing Synchrotron Radiation Facility (BSRF). This work was supported by the National Scientific Foundations of China (Grants 51702330, 11974360, 51872297, 51890864, 51802321, 21975132 and 21991143) and the Young Elite Scientist Sponsorship Program by CAST (YESS).

Conflict of Interest

The authors declare no conflict of interest.

Data Availability Statement

The data that support the findings of this study are available in the Supporting Information of this article.

Keywords: Borates · Hybridization Transformation · Ionic Crystal · Stress Transfer

- [1] a) W. L. Mao, H. K. Mao, P. J. Eng, T. P. Trainor, M. Newville, C. C. Kao, D. L. Heinz, J. F. Shu, Y. Meng, R. J. Hemley, *Science* **2003**, *302*, 425–427; b) S. Scandolo, M. Bernasconi, G. L. Chiarotti, P. Focher, E. Tosatti, *Phys. Rev. Lett.* **1995**, *74*, 4015–4018.
- [2] R. P. Dias, C.-S. Yoo, V. V. Struzhkin, M. Kim, T. Muramatsu, T. Matsuoka, Y. Ohishi, S. Sinogeikin, *Proc. Natl. Acad. Sci. USA* **2013**, *110*, 11720–11724.
- [3] M. J. Lipp, W. J. Evans, B. J. Baer, C. S. Yoo, *Nat. Mater.* **2005**, *4*, 211–215.
- [4] a) M. I. Eremets, A. G. Gavriluk, I. A. Trojan, D. A. Dzivenko, R. Boehler, *Nat. Mater.* **2004**, *3*, 558–563; b) V. Iota, C. S. Yoo, H. Cynn, *Science* **1999**, *283*, 1510–1513; c) C. S. Yoo, H. Cynn, F. Gygi, G. Galli, V. Iota, M. Nicol, S. Carlson, D. Hausermann, C. Mailhot, *Phys. Rev. Lett.* **1999**, *83*, 5527–5530; d) I. N. Frantsevich, T. R. Balan, A. V. Bochko, S. S. Dzhamar, G. G. Karyuk, A. V. Kurdyumo, A. N. Pilyanke, *Dokl. Akad. Nauk SSSR* **1974**, *218*, 591–592; e) C. S. Yoo, M. Nicol, *J. Phys. Chem.* **1986**, *90*, 6726–6731; f) T. Yagi, W. Utsumi, M.-A. Yamakata, T. Kikegawa, O. Shimomura, *Phys. Rev. B* **1992**, *46*, 6031–6039.
- [5] a) M. Akaishi, H. Kanda, S. Yamaoka, *J. Cryst. Growth* **1990**, *104*, 578–581; b) R. Z. Khaliullin, H. Eshet, T. D. Kuehne, J. Behler, M. Parrinello, *Nat. Mater.* **2011**, *10*, 693–697; c) T. Irifune, A. Kurio, S. Sakamoto, T. Inoue, H. Sumiya, *Nature* **2003**, *421*, 806–806.
- [6] a) Y. Shang, Z. Liu, J. Dong, M. Yao, Z. Yang, Q. Li, C. Zhai, F. Shen, X. Hou, L. Wang, N. Zhang, W. Zhang, R. Fu, J. Ji, X. Zhang, H. Lin, Y. Fei, B. Sundqvist, W. Wang, B. Liu, *Nature* **2021**, *599*, 599–604; b) H. Tang, X. Yuan, Y. Cheng, H. Fei, F. Liu, T. Liang, Z. Zeng, T. Ishii, M.-S. Wang, T. Katsura, H. Sheng, H. Gou, *Nature* **2021**, *599*, 605–610; c) S. Zhang, Z. Li, K. Luo, J. He, Y. Gao, A. V. Soldatov, V. Benavides, K. Shi, A. Nie, B. Zhang, W. Hu, M. Ma, Y. Liu, B. Wen, G. Gao, B. Liu, Y. Zhang, Y. Shu, D. Yu, X.-F. Zhou, Z. Zhao, B. Xu, L. Su, G. Yang, O. P. Chernogorova, Y. Tian, *Natl. Sci. Rev.* **2022**, *9*, 140–140.
- [7] C. T. Chen, T. Sasaki, R. K. Li, Y. C. Wu, Z. S. Lin, Y. Mori, Z. G. Hu, J. Y. Wang, G. Aka, M. Yoshimura, Y. Kaneda, *Nonlinear Optical Borate Crystals-Principles and Applications*, Wiley-VCH, New York, **2012**.
- [8] a) V. V. Brazhkin, Y. Katayama, K. Trachenko, O. B. Tsiok, A. G. Lyapin, E. Artacho, M. Dove, G. Ferlat, Y. Inamura, H. Saitoh, *Phys. Rev. Lett.* **2008**, *101*, 035702; b) S. K. Lee, P. J. Eng, H. K. Mao, Y. Meng, M. Newville, M. Y. Hu, J. F. Shu, *Nat. Mater.* **2005**, *4*, 851–854; c) S. K. Lee, P. J. Eng, H.-K. Mao, Y. Meng, J. Shu, *Phys. Rev. Lett.* **2007**, *98*, 105502; d) S. K. Lee, K. Mibe, Y. W. Fei, G. D. Cody, B. O. Mysen, *Phys. Rev. Lett.* **2005**, *94*, 165507.
- [9] Deposition Number 2116850 contains the supplementary crystallographic data for this paper. These data are provided free of charge by the joint Cambridge Crystallographic Data Centre and Fachinformationszentrum Karlsruhe Access Structures service.
- [10] a) E. Y. Borovikova, K. N. Boldyrev, S. M. Aksenov, E. A. Dobretsova, V. S. Kurazhkovskaya, N. I. Leonyuk, A. E. Savon, D. V. Deyneko, D. A. Ksenofontov, *Opt. Mater.* **2015**, *49*, 304–311; b) G. V. S. S. Sarma, C. V. Reddy, S. V. P. Vattikuti, C. R. Krishna, P. N. Murthy, R. V. S. S. N. Ravikumar, *J. Mol. Struct.* **2013**, *1048*, 64–68; c) S. N. Sofronova, Y. V. Gerasimova, A. N. Vtyurin, I. A. Gudim, N. P. Shestakov, A. A. Iyanenko, *Vib. Spectrosc.* **2014**, *72*, 20–25; d) C. L. Hayward, S. P. Best, R. J. H. Clark, N. L. Ross, R. Withnall, *Spectrochim. Acta Part A* **1994**, *50*, 1287–1294; e) A. Rulmont, P. Tarte, J. M. Winand, *J. Mater. Sci. Lett.* **1987**, *6*, 659–662; f) Y. J. Jiang, Y. Wang, L. Z. Zeng, *J. Raman Spectrosc.* **1996**, *27*, 601–607.
- [11] a) C. M. Julien, M. Massot, *Mater. Sci. Eng. B* **2003**, *97*, 217–230; b) S. Chakrabarti, A. K. Thakur, K. Biswas, *Ionics* **2017**, *23*, 1985–1993; c) M. Nocuñ, M. Handke, *J. Mol. Struct.* **2001**, *596*, 145–149.
- [12] C.-S. Yoo, *Matter Radiat. Extremes* **2020**, *5*, 018202.
- [13] J. Dong, Z. Yao, M. Yao, R. Li, K. Hu, L. Zhu, Y. Wang, H. Sun, B. Sundqvist, K. Yang, B. Liu, *Phys. Rev. Lett.* **2020**, *124*, 065701.
- [14] a) A. Brager, *Acta Physicochim. URSS* **1937**, *7*, 699–706; b) A. V. Kurdyumov, N. F. Ostrovskaya, A. N. Pilyankevich, G. A. Dubitskii, V. N. Slesarev, *Sov. Phys. Dokl.* **1976**, *21*, 402–403.
- [15] M. Marezio, J. P. Remeika, *J. Chem. Phys.* **1966**, *44*, 3348.
- [16] F. Occelli, P. Loubeyre, R. Letoullec, *Nat. Mater.* **2003**, *2*, 151–154.
- [17] M. Grimsditch, E. S. Zouboulis, A. Polian, *J. Appl. Phys.* **1994**, *76*, 832–834.
- [18] H.-Y. Chung, M. B. Weinberger, J. B. Levine, A. Kavner, J.-M. Yang, S. H. Tolbert, R. B. Kaner, *Science* **2007**, *316*, 436–439.
- [19] V. L. Solozhenko, D. Andrault, G. Fiquet, M. Mezouar, D. C. Rubie, *Appl. Phys. Lett.* **2001**, *78*, 1385–1387.
- [20] H. Cynn, J. E. Klepeis, C. S. Yoo, D. A. Young, *Phys. Rev. Lett.* **2002**, *88*, 135701.
- [21] X. Jiang, M. S. Molokeev, L. Dong, Z. Dong, N. Wang, L. Kang, X. Li, Y. Li, C. Tian, S. Peng, W. Li, Z. Lin, *Nat. Commun.* **2020**, *11*, 5593–5593.
- [22] a) E. Hirose, K. Kataoka, H. Nagata, J. Akimoto, T. Sasaki, K. Niwa, M. Hasegawa, *J. Solid State Chem.* **2019**, *274*, 100–104; b) A. Kuhn, E. Tobschall, P. Heitjans, *Z. Phys. Chem. (Berlin, Ger.)* **2009**, *223*, 1359–1377; c) P. Heitjans, E. Tobschall, M. Wilkening, *Eur. Phys. J.* **2008**, *161*, 97–108.
- [23] K. Toyoura, Y. Koyama, A. Kuwabara, F. Oba, I. Tanaka, *Phys. Rev. B* **2008**, *78*, 214303.
- [24] a) S. M. Eggins, R. L. Rudnick, W. F. McDonough, *Earth Planet. Sci. Lett.* **1998**, *154*, 53–71; b) M. Pertermann, M. M. Hirschmann, *J. Petrol.* **2003**, *44*, 2173–2201.

Manuscript received: June 6, 2022

Accepted manuscript online: September 9, 2022

Version of record online: September 29, 2022